ELSEVIER

Marine Geology 214 (2005) 431–449

MARINE GEOLOGY
INTERNATIONAL JOURNAL OF MARINE GEOLOGY, GEOCHEMISTRY AND GEOPHYSICS

www.elsevier.com/locate/margeo

Correlation of sidescan backscatter with grain size distribution of surficial seabed sediments

J.S. Collier[a,*], C.J. Brown[b,1]

[a]*Department of Earth Science and Engineering, Imperial College, University of London, RSM Building, Prince Consort Road, London SW7 2BP, UK*
[b]*Scottish Association for Marine Science, Dunstaffnage Marine Laboratory, Dunbeg, Oban, Argyll, PA37 1QA, Scotland, UK*

Received 23 February 2004; received in revised form 12 October 2004; accepted 5 November 2004

Abstract

The dependence of acoustic backscatter on sediment grain size distribution is examined using dual frequency (100 and 410 kHz) sidescan sonar and 22 sediment grab samples from the Loch Linnhe artificial reef site on the west coast of Scotland. The sidescan data were processed to remove an empirically estimated average grazing angle dependence on backscatter. The processed data were analysed by forming histograms of pixels extracted from a 20 m^2 box around each ground truth site. A positive correlation (r=0.73) between mean backscatter intensity and mean grain size was obtained, i.e., the coarsest samples had the brightest backscatter. A positive correlation (r=0.59) was also found between the standard deviations of the backscatter and grain size distributions, i.e., poorly sorted sediments gave the most variable backscatter. The performance of the sidescan data was compared to results from a co-incident single-beam echo-sounder RoxAnn survey. The RoxAnn roughness index E1 compared well with the sidescan, whilst the RoxAnn hardness index E2 did not. This may be due to a physical link between the acoustic measures. The comparison showed the sidescan to have delivered a significantly higher-resolution image of the seabed for a similar amount of ship-time. Imaging of the artificial reef modules themselves was found to be frequency dependent.

Keywords: sidescan sonar; seabed properties; sediment classification; RoxAnn; artificial reef

1. Introduction

1.1. Application of marine acoustic methods to quantitative site investigation

High-frequency sidescan sonar is routinely used in qualitative seabed mapping studies where the primary aim is to locate features and objects on the seabed. The success of the method is largely due to the fact that it

* Corresponding author. Tel.: +44 20 7594 6443; fax: +44 20 7594 7444.
E-mail addresses: Jenny.collier@imperial.ac.uk (J.S. Collier), c.brown2@ulster.ac.uk, craig.brown@sams.ac.uk (C.J. Brown).
[1] Present address: Centre for Coastal and Marine Research, School of Environmental Sciences, University of Ulster, Coleraine Campus, Cromore Road, Coleraine, Co. Londonderry, BT52 1SA, Northern Ireland, UK. Tel.: +44 2870 323337, +44 1631 559316; fax: +44 1631 559001.

0025-3227/$ - see front matter © 2004 Elsevier B.V. All rights reserved.
doi:10.1016/j.margeo.2004.11.011

provides rapid coverage over the ground using instruments that are widely available, affordable and relatively easy to operate from a range of different vessels. In these studies, the data are presented as black and white "sonic photographs" which are interpreted by eye. Data processing is generally restricted to geometric corrections required to geographically position the pixels and image enhancement—effectively to make the image "look good" by balancing backscatter intensity levels (Johnson and Helferty, 1990). The method works best for surveys where distinct seabed features (such as lava flows and faults) display characteristic backscatter responses. The visual interpretation of the sidescan images is generally guided by additional "ground truthing" of the seabed which may take the form of grab samples, cores or underwater photographs (Blondel and Murton, 1997). Advanced interpretation uses textural analysis techniques to more rigorously discriminate between defined seabed classes (e.g., Pace and Gao, 1988; Huvenne et al., 2002). A disadvantage with this type of approach is that in many situations, there is a gradual change in seabed type, without clear demarcations between backscatter behaviour. One of the goals of the current research, therefore, is to extend the quantitative interpretation of sidescan data to enable the direct extraction of specific seafloor properties such as mean grain size, sediment sorting, lithology, grain shape or porosity. These geotechnical parameters are particularly important for marine construction and environmental studies in shallow water.

Seabed acoustic imagery may contain (i) specular (true) reflections and acoustic shadows generated at the seabed as well as (ii) backscatter from seabed irregularities (surface scattering) or from heterogeneities within the near-surface sediments (volume reverberation, Urick, 1967). A major obstacle to interpreting the imagery is that the physics of scattering is complex and not fully understood (Jackson et al., 2002). It has even proven problematic to numerically model the measured backscatter response of well-characterised sediments made under highly controlled field conditions (Williams et al., 2002). However, it is known that the backscattering phenomena are related to seabed roughness or volumetric heterogeneity on scales similar to that of the incident wavelength and have a grazing angle dependence (Gardner et al., 1991; Jackson et al., 1986). Surface roughness or internal heterogeneity may be directly related to grain size or other factors such as sedimentary structures, bioturbation or gas bubbles (Urgeles et al., 2002; Fonseca et al., 2002). For real seabeds, the situation is further complicated if bedforms such as ripples change the local grazing angle and so cause an azimuthal dependence on the surface backscatter (Bell et al., 1999). For volume scattering, the backscatter intensity level is also influenced by the depth of penetration of the signal, which is a function of acoustic attenuation of the sediment and the acoustic frequency (Stanton, 1984; Jackson et al., 1986). In theory, volume scattering should not occur beyond the critical angle (total internal reflection occurs), but in practice, significant returns have been recorded at these larger angles (Jackson et al., 2002).

Recently, there has been some success in the development of commercial seabed classification systems using conventional single beam, vertical-incidence echo-sounders (collectively known as 'Acoustic Ground Discrimination Systems', AGDS). One such system, RoxAnn™ (Stenmar Microsystems, Aberdeen) uses analogue signal processing hardware to extract two indices from the echo return (Burns et al., 1985; Chivers et al., 1990)—the envelope of the decaying return after the initial peak, termed E1, and the entire first multiple reflection, E2 (Fig. 1). The first and last point in each of the integrals is calculated automatically by a logic control circuitry. A rougher surface is expected to have a lower initial peak and a longer tail than a smoother surface of the same composition (acoustic impedance), hence, E1 is sometimes known as " roughness" (Hamilton et al., 1999). Similarly, a hard seabed (high acoustic impedance) reflects a greater proportion of the incident energy making the second echo stronger than a soft seabed, hence, E2 is sometimes known as "hardness". During surveying, E1 and E2 are displayed on a Cartesian *XY* plot, and different regions on the graph assigned to user-defined seabed classes. Despite the ad hoc method of classification, the system represents a step-forward in the automatic classification of seabed type and has the advantage that it can be conducted in real time by a range of operators. Accuracy in the seabed classification (when compared to ground truth results) as high as 80% has been reported (e.g., Pinn and Robertson, 2003). The raw data can also be exported for post-processing and more sophisticated image classification

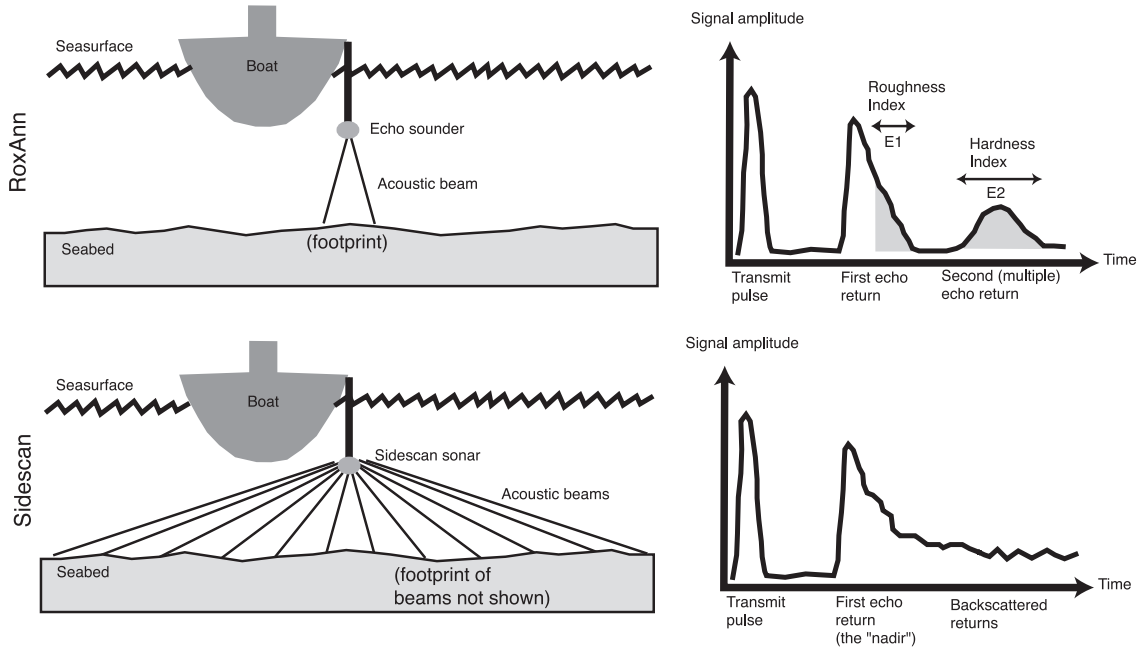

Fig. 1. Cartoon showing the different acquisition geometries and signal records of RoxAnn and sidescan.

using supervised and unsupervised classification techniques (e.g., Sotheran et al., 1997; Greenstreet et al., 1997; Foster-Smith and Sotheran, 2003). The largest technical problem with RoxAnn appears to be in the measurement of the second echo strength, E2. Previous studies have reported correlations between E2 and ship speed, presumably due to a significant reduction in the reflection coefficient of the sea-surface around the vessel as it travels faster (Schlagentweit, 1993; Hamilton et al., 1999).

Sidescan sonar operates by emitting a fan or swathe of acoustic energy (Fig. 1). Data are therefore collected over a wide range of grazing angles, with a single grazing angle measurement at any point on the seabed. Therefore, although the method has a great advantage over single beam methods that data is collected from most of the seabed (without the need to interpolate between tracks) and the acoustic footprint on the seabed is generally much smaller, it has the disadvantage that the measurements are not made with the same insonification geometry (Hughes-Clarke, 1994). In this study, we attempt to correct for the grazing-angle dependence on backscatter by empirically estimating it from field data and removing it. This requires us to assume that the acoustic properties of the seabed sediments within our small study area do not vary significantly. We use a field dataset typical of a mid-budget site investigation, collected with a commercial dual frequency sidescan fish. Our dataset has a number of limitations, and is subject to the usual problem of water column noise associated with towed instruments. We assess the success of our analysis by comparing the processed sidescan backscatter data to sediment grain size distributions from ground truth samples. In addition, we compare the sidescan results against those obtained from a normal-incidence RoxAnn study. In the mainstream literature, there are few examples comparing sidescan and RoxAnn surveys (Collins and Voulgaris, 1993, being an exception). The overall aim of our work was to assess the potential of sidescan for automatic ground discrimination. The method has several advantages over single-beam work in terms of spatial coverage and resolution, yet, it needs to be demonstrated that robust quantitative results can be extracted.

1.2. The study area

Loch Linnhe is a sea loch formed within the Great Glen Fault, one of the major NE–SW Caledonian

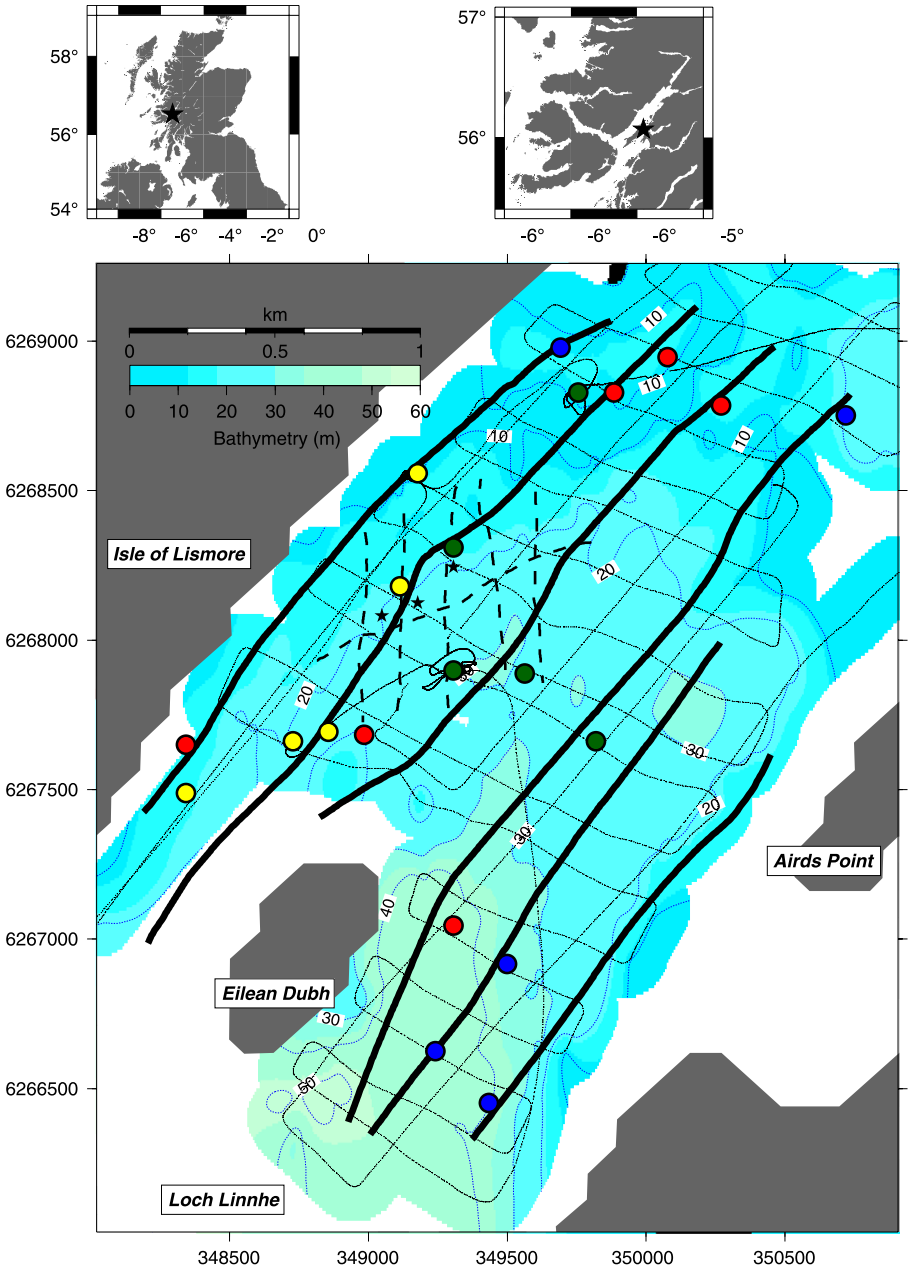

Fig. 2. Maps of study area (star in small maps), land is shaded mid-grey. Large map shows details of survey, bold lines are 100 kHz sidescan sonar tracks, dashed lines 100/410 kHz sidescan sonar tracks and fine dotted lines single-beam echo sounder tracks. All navigation was via dGPS, with an estimated accuracy of 5 m. The scale in this, and all subsequent plots, is UTM metres. Bathymetry measurements were reduced to Admiralty Chart Datum (OD) using tide gauge measurements at Tobermory, Mull, binned into 20 m cells using a median filter and gridded using a tensioned minimum curvature surface (Smith and Wessel, 1990). Stars show artificial reef locations and the coloured dots are sediment sample stations coded by mean grain size—with red (Φ_{mean}<3.5, stations with coarsest sediments), green, (4.25>Φ_{mean}>3.5), yellow (5>Φ_{mean}>4.25) and blue (Φ_{mean}>5, stations with finest sediments).

structures that define the geology of Scotland (Fig. 2). The Fault juxtaposes Pre-Cambrian Moine metasediments to the north and Late Pre-Cambrian Dalradian metasediments to the south. The southeast shore and the island of Lismore within the loch itself consist of Dalradian quartzites, slates and limestones (Fyfe et al., 1993). The northwest shore of Loch Linnhe includes a Caledonian Granite pluton and some Mesozoic and Cenozoic sedimentary outliers, together with the Moine sequence. These rocks provide a very mixed provenance, with highly variable weathering and erosional characteristics.

The region was actively glaciated during the Quaternary. Moraines, exposed striated bedrock and dropstones have been discovered offshore (Fyfe et al., 1993). Beyond Mull, there are thick glaciomarine sediments deposited within low resistant bedrock. Today, the near-shore regions are characterised by muds with variable coarse components that are reworked glaciomarine sediments. Recovered gravel clasts around the Isle of Mull are predominantly garnet–mica schists from the Moine series. Although global sea-level fell by more than 100 m during the most extensive glaciations, here, ice loading caused a relative sea-level rise with raised beaches 40–70 m above OD found along the coast. Following glaciation the region has experienced isostatic uplift, which continues today at a rate of ~2 mm/year (Shennan, 1989).

Dunstaffnage Marine Laboratory was licensed to deploy experimental artificial reefs within Loch Linnhe in 2001 (Sayer and Wilding, 2002). The project will assess various reef designs for potential economic return from reef-based fisheries for the European Lobster (*Homarus gammarus* (L.)). Foster

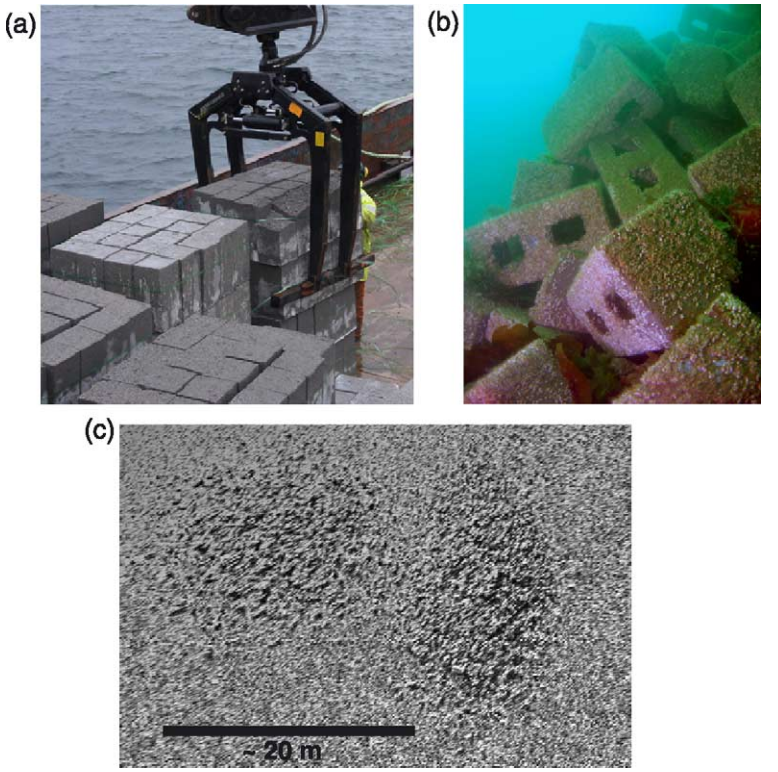

Fig. 3. (a) Photographs of artificial reef blocks being deployed from the MV Rose of Lorne. Two types of block are used for reef construction—solid ones as shown here and ones with cavities as shown in the next photo. Individual blocks measure 40×20×20 cm. (b) Underwater photograph of reef blocks in situ on the seabed. This photograph was taken about 6 months after the deployment and sidescan imagery and shows the rapid pace of colonization by marine epifauna. (c) Raw 410 kHz sidescan image of one of the reef sites. White is high backscatter and black low backscatter. The image clearly shows two distinct piles of coarse texture generated by a small alignment error of the vessel during successive block deployment episodes.

Yeoman, the industrial partners on the project, are currently producing two types of concrete blocks for use in the construction of the reef complex from by-products from their coastal granite quarry at Glensanda on the Morvern Peninsula, to the north of Loch Linnhe. The blocks (which measure 40×20×20 cm) are deployed by crane from a barge and free-fall to form discrete mounds or modules on the seabed in water depths between 15 and 25 m (Fig. 3). The complex will be made up of 42 reef modules of two sizes with an overall weight of up to 25,000 tonnes in total (Sayer and Wilding, 2002).

The physical introduction of the reef modules will significantly alter the biological habitat characteristics of the area. The change in the proportion of hard to soft seabed types and the height of the seabed may alter existing current profiles and so lead to changes in sediment profiles in the surrounding area. All of these physical changes are likely to have consequences for both the existing biological communities and what may develop post-construction (Wilding and Sayer, 2002). The variety and range of habitat manipulation within the artificial reef complex will enable the environmental effects of different construction types to be modelled and assessed.

The sidescan survey presented here took place over 2 days in March 2002, when three of the reef modules were in the early stages of construction. The survey had two aims, firstly to determine the in situ shape of the reefs to help subsequent block deployments achieve optimal reef design, and secondly to determine the distribution of seabed sediments at the start of construction. The interpretation of the benthic biodiversity and correlation with seabed type is presented elsewhere (Brown et al., 2002; Brown, in preparation).

2. Methods

2.1. Single beam echo sounding

The RoxAnn system used in this study was attached to a Furuno, 200 kHz single beam echo sounder. The echo sounder, which was rigidly mounted to the side of the R/V *Seol Mara*, has a 10° beam angle, giving a 19 m^2 seabed footprint in a water depth of 30 m. A survey grid of lines 300–400 m apart navigated with differential GPS was completed in 6 h during a single day in April 2002. The track lines and the tidally corrected bathymetry are shown in Fig. 2. In the centre of the Loch, there are small islands and submerged rocky outcrops (not imaged). Otherwise, the bathymetry was found to be rather featureless, and gently deepening to 52 m towards the southeast of the study area. The RoxAnn indices E1 and E2 values were binned into 20 m cells, averaged and fitted with a mesh surface using GMT software (Wessel and Smith, 1991).

2.2. Sediment grain size analysis

Sediment samples and under-water video were collected at 22 stations during April 2002. A 0.1 m^2 Hamon grab was used to collect benthic samples for geological and biological analysis. Sampling stations were randomly positioned across the survey area. Replicate grab samples (four in total) were taken at six of the stations to assess the repeatability of the sampling method. On the basis of water depth, wire angle and sea conditions, we estimate the positional accuracy of individual grabs to be ±15 m. Following estimation of the total volume of each grab sample, a 500 ml sub-sample was removed for laboratory particle size analysis. The remaining sample was washed over 5 and 1 mm square mesh sieves to remove excess sediment. The retained macrofauna were fixed in 4–6% formaldehyde solution (diluted with seawater) for laboratory identification and enumeration (not reported on here).

Sediment particle size analysis was conducted on each 500 ml sub-sample following standard protocols described by Boyd (2002). Fine material content (mud, silt and sand) was determined with a laser sizer. The remaining material from each 500 ml sub-sample was dried, weighed and sieved through a 2 and 4 mm mesh. The results from the fine and coarse analyses were then combined to give the percentage weight per Wentworth (phi) grain size class for each grab sample. Note that the Wentworth scale ($\Phi = -\log_2 d$, where d is diameter of grain in mm) is inverted, i.e., fine sediments have large Φ values. Finally, the mean grain size (Φ_{mean}) for each station was calculated by averaging the individual percentages for each grain size bin.

2.3. Sidescan sonar

The survey used a dual frequency (100 and 410 kHz, wavelengths 15 and 4 mm, respectively, ping rate 6 Hz) GeoAcoustics 159D sonar towed at 2–3 knots, about 1.5 m below the water line from a 3 m pole mounted on the starboard quarter of the R/V *Calanus*. Theoretically, the sonar has a minimum across-track resolution of 4 cm (calculated assuming a pulse band-width of the instrument of 20 kHz, Somers and Stubbs, 1984) and minimum along-track resolution of ~10 cm (calculated assuming a horizontal beam width of <1°). Resolution tests using data collected over a shipwreck with distinctive features of known dimension suggested that the practical minimum across- and along-track resolutions were 10 and 20 cm, respectively, for the survey parameters used here.

The main survey was conducted at 100 kHz (Fig. 2). Near-complete sonar coverage within the study area was achieved with a pattern of NNE–SSW-orientated, parallel survey lines spaced approximately 200 m apart. This survey took approximately 5 h to complete. Additional sidescan profiles were collected around the artificial reefs at both 100 and 410 kHz in a N–S and NE–SW line orientation. Unfortunately, during the high-frequency survey, interference with the vessel was recorded which degraded the image of the inner half of the port swathe. The rest of the data, however, was recorded without any noticeable contamination. The boat was navigated by real-time differential GPS. Some deviations in the ship tracks were needed to avoid submerged rocks and tethered buoys used to surface mark the artificial reef sites. A navigational fix of the vessel was logged every second, with interpolated positions written into the headers of each sonar ping. Additional positioning or movement sensors on the towed sonar were not available, so the fish is assumed to follow the path of the vessel (with a single offset and layback from GPS antenna correction) and without any correction for pitch, roll or yaw. The sea-conditions were unusually calm during the survey period and tow conditions optimally smooth.

Within the sidescan hardware, there is an analogue time-varying amplification to correct for transmission loss (geometric spreading and water-column attenuation). The system's default mode of operation is to also apply additional analogue gain functions (agc) that vary during the course of the survey to produce a "balanced" visual image. Here care was taken to record the "raw backscatter" data without any additional system gains to allow the quantitative analysis to be performed. The raw amplitude pixel data were digitally recorded as integer numbers with 11 bits, giving grey levels from 1 to 2047. The sonar is uncalibrated (unknown source level and radiation patterns), so backscatter intensity values that follow are presented in relative integer values rather than dB. An insignificant percentage (<0.02%) of the data were recorded clipped. The background noise level, estimated from pixel values in the water column away from the sea-surface ship's hull reflection, was <30.

The raw sidescan sonar data files were transferred to a UNIX workstation for processing using in-house software developed at Imperial College (Humber, 2003). The approach taken follows the digital methods developed for seafloor geology mapping studies (e.g.,

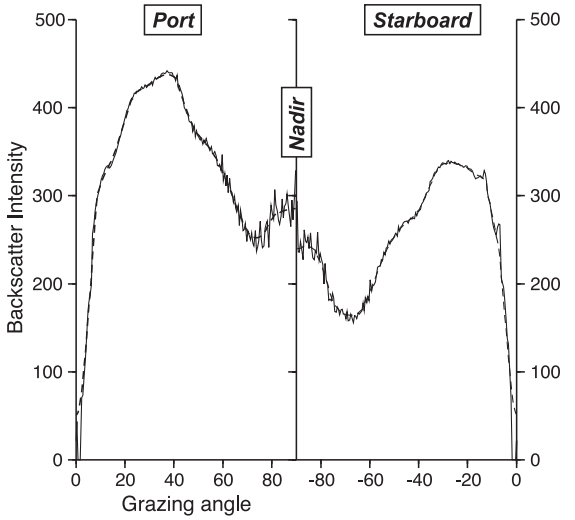

Fig. 4. Average across-track pixel values for the main 100 kHz loch survey. Pixel values with common grazing angles from the inner four swathes were averaged. Data from the two profiles closest to the shoreline were excluded from the averaging, as the 2D bathymetric assumption would give unreliable grazing angle estimates. Note that in sidescan datasets grazing angles are biased towards acute angles (as they are sampled in slant-range) so the estimate of average backscatter is least accurate close to the nadir (this contributes to the apparent noisiness of the plot here). The dashed line shows the smoothed version of the amplitude trend used to normalise the data.

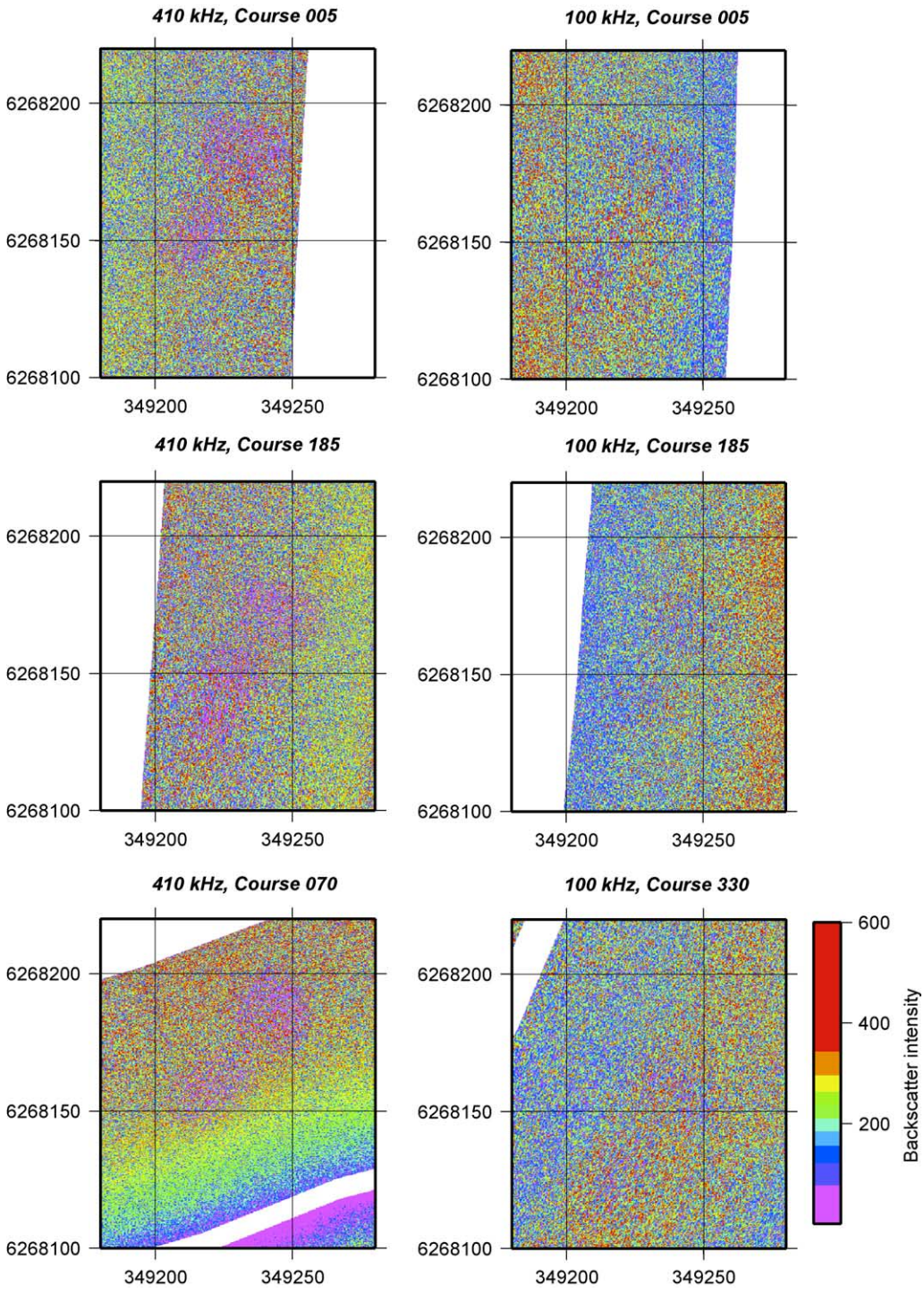

Fig. 5. Comparison of sidescan images of the same artificial reef module (consisting of two piles of blocks) for different frequency and look-angle (ship course). The coarse structure of the reefs is well imaged on the 410 kHz images (where they have relatively low backscatter intensity and appear pink), but poorly imaged on all the 100 kHz ones. Comparison of the locations of the piles shows the navigational error of the sidescan to be ~20 m.

Chavez, 1986; Cervenka and de-Moustier, 1993; Blondel and Murton, 1997). Water sound velocity measurements made in the Loch showed it to be well mixed (Vp=1495 m/s), and straight line propagation through the water column was assumed throughout. The first stage in the processing sequence was to edit out data collected during boat turns. The seabed reflection was then manually picked to give an estimate of fish altitude along the ship track. Subsequent processing used this altitude combined with a flat-seafloor assumption to give the grazing angle of each pixel across the swath. This assumption was considered reasonable given the gentle bathymetry (maximum slope 3°) and likely scale of grazing angle errors due to unknown fish motion. The dataset shows no evidence for small-scale bedforms such as ripples, and data collected at different look-angles appear uniform. We therefore assume that directivity can be ignored here. The data was then slant-range corrected and re-sampled to give pixels evenly spaced in ground-range. The inner 10 m of the swath (the nadir) was zeroed as this portion of the record is dominated by reflection giving anomalous amplitudes.

The raw data contained clear, long-wavelength across-track amplitude variations. This amplitude trend was estimated by averaging pixel values with common grazing angles, an example of which is given in Fig. 4. The amplitudes show different port and starboard transmit and receiver array beam patterns (the port side values being consistently higher). Most of the amplitude trend is likely to be caused by the main and side lobes of the linear beam array. Superimposed on the instrument beam pattern will be any seabed grazing-angle backscatter dependence. The amplitude minimum at a grazing angle of ~70° correlates with the estimated critical angle for the sediments (see Results) and so may correlate with a change in the volumetric and surface scattering behaviour. To correct for the long-wavelength amplitude trend, pixels were multiplied by the inverse of a smoothed version of the average across-track beam amplitude trend. Note that this correction should remove any systematic seabed grazing-angle backscatter dependence.

The final stage in the process was to geographically register each pixel. Firstly, a cubic spline was fitted to the raw navigation data and it was re-sampled to one point every 5 s to remove small irregularities which translate into undesirable stretching and bunching of the pixels. The dataset was then geographically rectified using algorithms taken from the image processing software ER-mapper. During this process, the geographic latitude/longitudes were converted to UTM metres with a WGS-84 datum. The multiple passes over the three artificial reef sites allowed an estimate of the positional error to be made (Fig. 5). Overall, we estimate the maximum error in seabed position in the final processed sections to be 20 m. This error was larger than expected given that the navigation was via DGPS. It is possible that the strong tidal currents in Loch Linnhe (which has a tidal range of about 4 m) and ship manoeuvres to avoid tethered buoys significantly changed the tow position of the fish between passes. A composite image or mosaic was then made by merging the rectified grids for each swathe. It was decided not to implement a sophisticated mosaicing scheme, e.g., one that would allow user-selected parts of the image to be used in overlapping regions. The aim here was to preserve amplitudes for quantitative analysis rather than optimise for aesthetic appearance. There was also the realisation that the resolution of the data far exceeded the positional accuracy. For the final mosaics, pixels within overlapping zones were simply averaged. Subsequent numerical analysis was performed on the individual swathes.

3. Results

3.1. Loch sediments

The spatial distribution of the mean grain size throughout the study area is shown in Fig. 2. The loch sediments consist of silty muds with variable amounts of sand and gravel. Overall, the sediments fine towards the southeast. This trend was confirmed by the video footage and previous diver observations taken in the loch. Fig. 6 shows the grain size distribution for two of the repeat sample stations. The two stations shown have the highest and lowest variation in results for the repeat stations. Some of the variation will be positional error and some sampling error. In particular, the graphs illustrate the problem with accurately quantifying the coarsest sediment fraction (Φ<−1) via laboratory analysis. This poten-

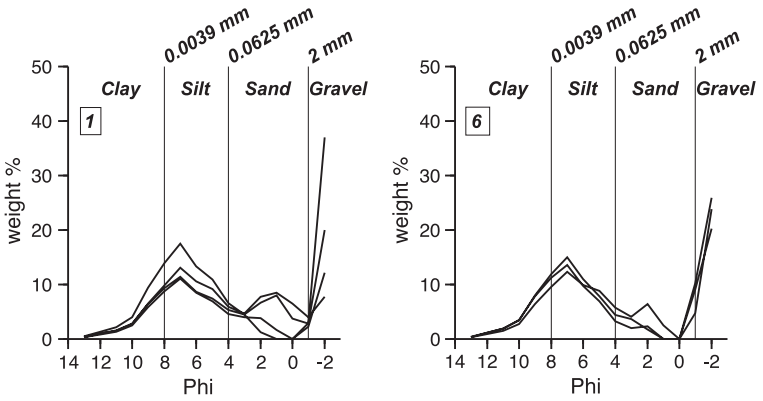

Fig. 6. Difference in sediment grain size analyses from repeat grabs at a particular station. The two stations illustrated were chosen as they have the most (station 1) and least (station 6) grain size variation of the six sites where duplicate grabs were taken. The locations of the ground truth sites are given in Fig. 8. We estimate from the spread of values that the minimum error in the calculation of the mean grain size at station 1 is $\pm 1.2\Phi$, and at station 6 is $\pm 0.3\Phi$. Similarly, we estimate the minimum error in the calculation of the standard deviation at station 1 is $\pm 0.4\Phi$, and at station 6 is $\pm 0.2\Phi$.

tially adds uncertainty to our study as the coarsest sediments may have a disproportional effect on the backscattered response.

As a guide to understanding the sidescan data, we estimate acoustic properties using the relationships given by Sternlicht and de-Moustier (2003). The average critical angle (where total internal reflection occurs) for the loch sediments calculated by this method is 22°, with a range of values between 18° and 24° for the various sediment types. Acoustic attenuation is estimated to range between 0.8 and 0.2 dB/m/kHz. At the frequencies used in our study (100, 200 and 410 kHz), this indicates a halving of signal strength for every 25–100 cm of travel into the sediment. The acoustic data collected therefore is providing information on sediments up to a couple of metres below the seabed.

3.2. The 100 kHz Loch Linnhe sidescan mosaic

The 100 kHz mosaic is shown in Fig. 7. In general, the backscatter intensity is highest in the north (orange/yellow colours), and reduces southward (through green/blue to blue colours), although there are distinct high-backscatter patches in the south. In the centre of the image (349 500, 6 268 000) is the anomalous reflection and acoustic shadows from the submerged Branra rock (ensonified from the west). Reflection banding parallel to the coastline of Lismore Island and the mainland is also seen on the outermost two swathes. Minor acquisition artefacts remain throughout the dataset. For example, there is occasional high-frequency along-track banding on the outermost parts of some of the more eastern swathes (e.g., near 350 000, 6 267 500), presumably due to fish motion. There is one electronic noise burst (shown by a narrow orange across track stripe) in the north extreme of the survey. However, more significant than acquisition artefacts is the fact that the across-track intensity correction did not work perfectly, giving track parallel striping in places. This imbalance appears to be systematic—in the high backscatter area in the north, it is characterised by a low intensity (blue) strip beyond the near-nadir region, whilst in the south, it is characterised by a higher (green/yellow) strip at a similar across-track location (note that in the deeper water in the south a pixel with a given grazing angle will be farther away from the nadir than in the north). Comparing raw sidescan across-track amplitude trends computed for regions of known sediment type suggested that for the gravelly sediments the amplitude minimum was at ~50 lower grazing angle than both the sandy and muddy sediments. The number of ground truth locations was not thought sufficient to investigate this effect further, but it is likely that where the sidescan shows track parallel striping the seabed sediments have different grazing-angle-dependent acoustic properties to the "average" properties used in processing.

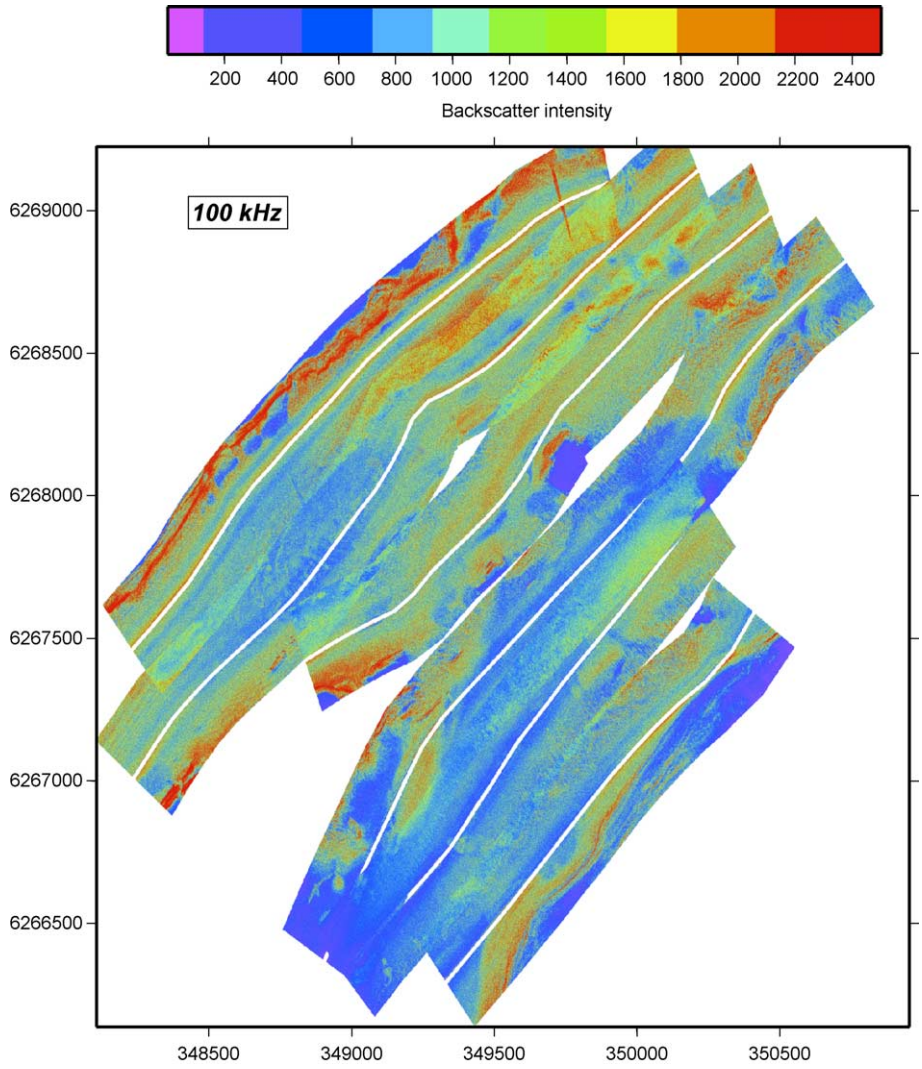

Fig. 7. The 100 kHz sidescan mosaic. The data are gridded into 50 cm bins. Each backscatter colour class represents 10% of the total pixels. The white line up the centre of each of the six swathes is the blanked nadir region.

3.3. Correlation between sidescan and RoxAnn indices

A contour map of the RoxAnn parameter E1 is shown in Fig. 8. Visually, this parameter appears to correlate with the sidescan mosaic. Overall, for example the higher sidescan backscatter in the north of the survey area coincides with high E1, and some of the shorter wavelength features of the sidescan grid, such as two distinct tongues of high backscatter (at 349 100, 6 267 000 and 350 100, 6 267 700) correlate with local RoxAnn highs. Not surprisingly, given the different seabed sampling (single versus multibeam), there is generally more detail in the sidescan image, for example a complex high sidescan backscatter feature at 348 900, 6 266 600 on the southeast shore of Eilean Dubh is seen in the RoxAnn image as poorly defined local 0.2 high. Some features seen in the RoxAnn E1 grid do not correlate with the sidescan image. The most significant of these are the small, high amplitude bull's eyes (E1>0.8) in the northern part of the survey. These were not thought to be

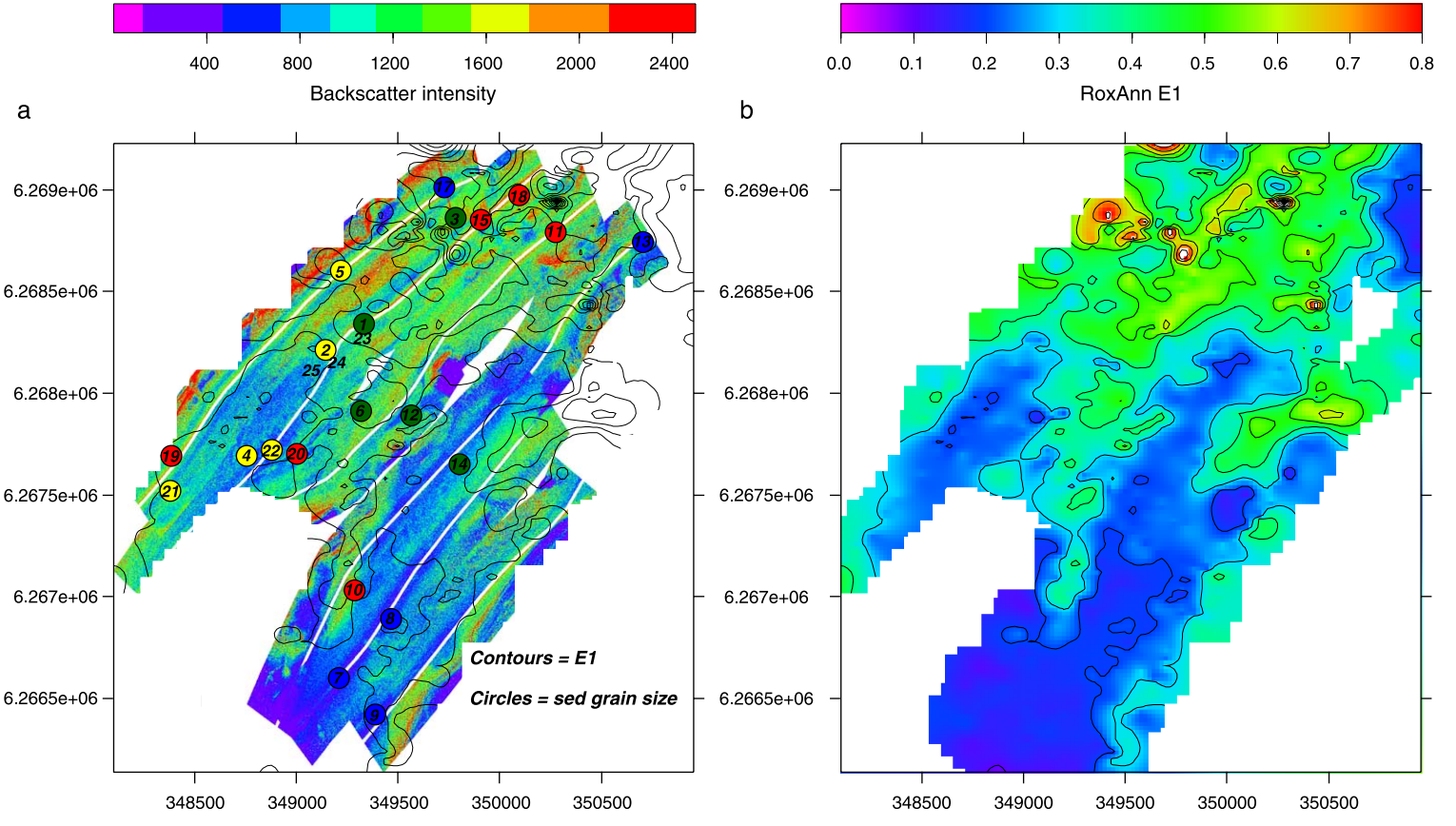

Fig. 8. Comparison of the 100 kHz sidescan (grid size 50 cm) with RoxAnn E1 (grid size 20 m). (a) Sidescan mosaic (as shown in Fig. 7) with RoxAnn E1 contours overlaid. Coloured dots are sediment sample stations (as numbered) colour coded to the same scale as Fig. 2. (b) RoxAnn E1 contours. Note the correlation between high backscatter and high E1.

gridding artefacts, but more likely due to erroneous RoxAnn values of unknown cause.

To test the robustness of the apparent correlation between the sidescan and RoxAnn E1 datasets, values were extracted from the two grids and plotted against each other (Fig. 9). Note that this graph only contains values extracted at the positions of the single beam ship tracks to avoid additional error due to interpolation between the ~100 m echo sounder tracks. To improve the signal to noise ratio of the sidescan, the data were regridded into 5 m bins. Despite these efforts to reduce scatter, the correlation between backscatter intensity and E1 is rather diffuse, and the correlation coefficient only 0.58. The correlation seems to be better defined at low E1. The RoxAnn parameter E2 did not appear to correlate with backscatter intensity either visually when the datasets were overlain, or when plotted against each other (Fig. 9, correlation coefficient 0.28). It is possible that there is an physical link between the E1 (roughness) index and backscatter that is not present between the E2 (hardness) index. Alternatively, the lack of correlation could be due to problems recording E2, which is very sensitive to ship speed (because of the effect this has on the seasurface reflectance) and ship roll (E2 generally took longer to stabilise after a roll than E1, because of its longer raypath geometry).

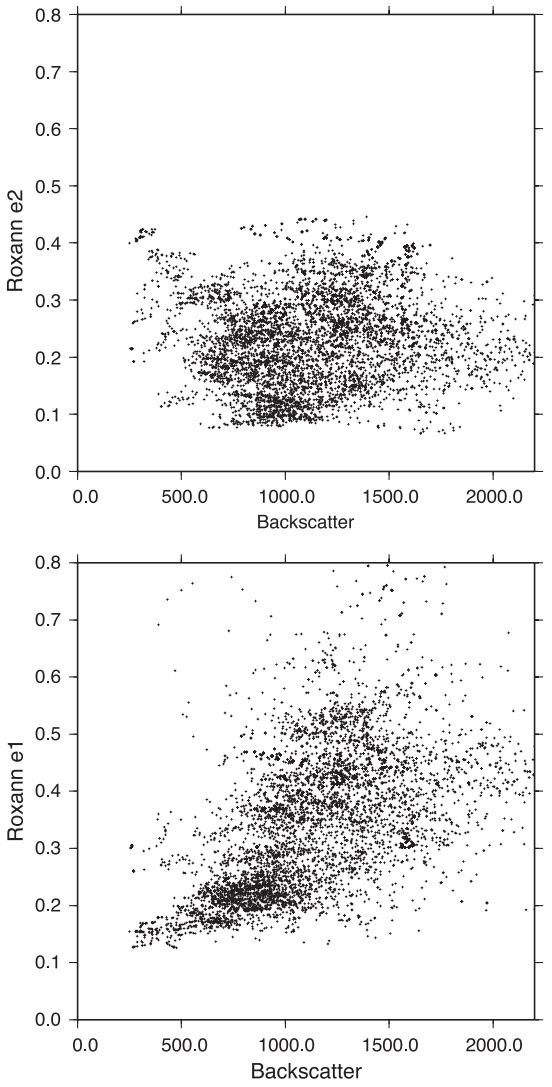

Fig. 9. Graphs of 100 kHz backscatter intensity against RoxAnn E1 and E2. Backscatter intensity was extracted from the final mosaic grid shown in Fig. 7 along the single-beam echo sounder tracks shown in Fig. 2.

3.4. Correlation between backscatter intensity and sediment grain size

To investigate the relationship between backscatter intensity and sediment grain size, pixels were extracted from the sidescan grid within 20×20 m boxes centred about each ground truth station. This box size was chosen to be comparable with the expected navigational uncertainties. In total, there were 20 useable co-incident grain size and backscatter locations, with a random set of sidescan grazing angles. The grain size and backscatter pixel intensity distributions were then plotted as histograms and statistics (mean and standard deviation) calculated. Graphs of the statistics for the sediments plotted against sidescan are shown in Fig. 10. This figure also shows complete histograms typical of the four main sediment types in the loch.

The mean sediment grain size has a positive correlation (r=0.73) with the mean backscatter intensity, with the coarsest sediments (low Φ_{mean}) having the highest mean backscatter. There is one significant outlier, station 11, which recorded by far the highest proportion of gravel—67% weight. The poor correlation with backscatter suggests there was a sampling error of the coarsest fraction, in this case that the true gravel content was less than measured in the lab. Otherwise, the correlation appears robust, and suggests that mean backscatter intensity could be mapped

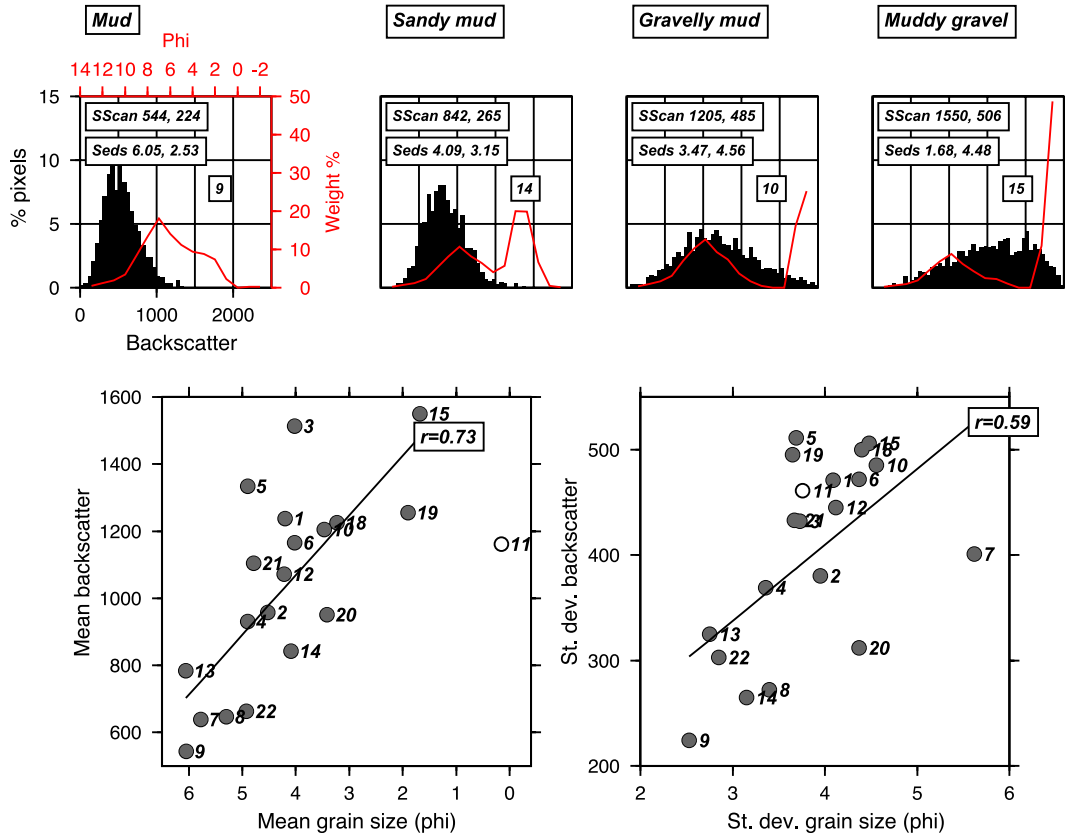

Fig. 10. Top: Comparisons between 100 kHz backscatter histograms (black filled, bottom and left axis) and sediment grain size distributions (red line, top and right red axes) for four typical stations. The axes are identical for the four plots. The four stations are arranged left-to-right in order of increasing coarseness. The boxes show mean and standard deviation values for the sidescan and sediment grain size distributions. Bottom: Graphs of 100 kHz sidescan pixel histogram versus sediment grain size statistics for all stations (as numbered, see Fig. 8 for locations). Best-fit linear regression straight lines are shown. We have not added error bars, but from the analysis of repeat grabs the uncertainty in the mean sediment grain size could be as high as 1.2Φ, and in the standard deviation $\pm$0.4Φ (see Fig. 6). (For interpretation of the references to colour in this figure legend, the reader is referred to the web version of this article.)

directly into mean sediment grain size. The standard deviation measurements also show a reasonable linear correlation—the stations that have the most poorly sorted sediment (large σ) generally have the broadest sidescan backscatter histograms. This correlation is well illustrated in the examples shown in Fig. 10, station 9, which has the most unimodal sediment grain size distribution and has a narrow sidescan pixel histogram, whereas station 15 which has a bimodal sediment grain size distribution has a broad sidescan pixel histogram. The phenomenon may be due to the more mixed sediment areas having a greater range in local grazing angles which is giving the increased variation in the recorded backscatter.

3.5. Acoustic properties as a function of frequency

Visual comparisons between the co-incident 100 and 410 kHz sidescan data suggested there to be little difference in the acoustic response of the Loch sediments at these two frequencies. This is in marked contrast to the artificial reef modules themselves that showed up as clear high and low backscatter regions in the 410 kHz imagery, but were poorly defined in the 100 kHz records (Fig. 5). The reason for this was unclear, but given that the corresponding acoustic wavelengths of 15 and 4 mm, respectively, are both significantly smaller than the deci-centimetre-scale concrete blocks presumably the roughness of the

blocks themselves is the cause. The lack of a detectable frequency dependence for the regular loch sediments is illustrated in Fig. 11. Note that because of the distribution of useable 410 kHz sidescan data and sediment-sampling stations, it was not possible to compare the 410 kHz data directly with the sediment grain size distributions, as was the case for the 100 kHz dataset. Therefore, we compare the sidescan records directly. Pixels were extracted within 20×20 m boxes at 15 randomly selected points around the artificial reef site. Each sample location had sidescan imagery at two different look-angles for both 100 and 410 kHz (i.e., there were four swathes used for each, and the grazing angles were variable and random). The graph of mean backscatter intensity shows a strong positive linear relationship, i.e., the sub-sampled areas of seabed that recorded high intensity backscatter at 100 kHz also gave high backscatter intensity at 410 kHz. It is possible that the dual frequency coverage did not sample sufficient sediment variation, and that if the 410 kHz survey had encompassed the silty muds in the south and the gravelly silty muds in the north, a frequency-dependent trend may have emerged. A frequency-dependent response might have been expected given that the high frequency wavelength is comparable with the coarse clasts in the loch, whilst the low-frequency wavelength is much bigger than the seabed clasts. Attempts were made to look for statistical relationships to discriminate between the responses to the two frequencies. The most promising relationship is also shown in Fig. 11, where the mean and standard deviations of the pixels within the 20×20 m boxes are compared. Without ground truthing, however, it is not possible to determine whether the different behavior of the two frequencies is a function of seabed or sidescan instrument properties.

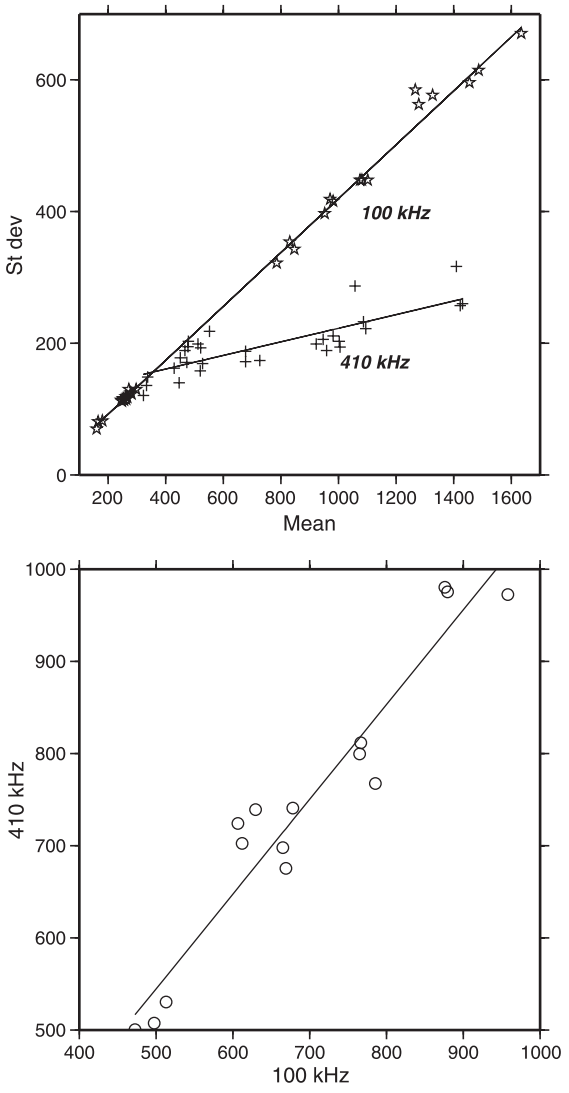

Fig. 11. Bottom: Graph of seabed backscatter intensity within randomly selected 20×20 m boxes recorded at 100 and 410 kHz. The seabed within the area studied does not seem to show a simple frequency-dependent backscatter intensity behaviour. Top: Graph of mean and standard deviations for the same dataset used in the lower graph. Stars are 100 kHz and crosses 410 kHz measurements. The two frequency populations appear to separate suggesting that there may in fact be some frequency dependency on the backscatter behaviour of the sediments.

4. Discussion

4.1. The correlation between backscatter intensity and sediment grain size distribution

As application of acoustic backscatter methods for quantitative seabed characterization is an emerging field, and there are arguably too few published studies so far to assess whether the empirical results obtained here are site-specific or more widely applicable. Most of the earlier studies have noted a positive correlation between backscatter strength and sediment grain size in general terms, i.e., that the highest backscatter correlates with the coarsest sediments (e.g., Knebel et

al., 1999; Edwards et al., 2003). However, Borgeld et al. (1999) and Urgeles et al. (2002) report a negative relationship between backscatter intensity and mean grain size. Both these studies incorporated flood deposits, and the high backscatter in the fine-grained sediments was attributed to anomalous internal stratigraphy and degree of bioturbation. To date, only a very few of these earlier studies have attempted to quantify the relationship between backscatter intensity and mean sediment grain size. The results from our work are in general agreement with available previous accounts (Davis et al., 1996; Ryan and Flood, 1996; Goff et al., 2000), which also suggested a simple "linear" relationship between the two parameters and we believe our results lend support to the potential of extracting seabed properties directly from digital sidescan data. However, to ensure a more robust use of sidescan data, it would be desirable to improve the correlations obtained between backscatter and sediment grain size properties. Further studies are needed to determine whether the scatter in the results could be reduced by improving field practices (such as positional accuracy of the sonar fish and sediment grab) or processing methods (such as using 3D bathymetry to more accurately determine the grazing angle of each pixel, or developing a more sophisticated way to compensate for the grazing-angle dependence on backscatter for different sediment types). Alternatively, the moderate degree of correlation between measured backscatter and sediment grain size properties obtained in this study may be inherent due to the natural local variability of surficial sediments and the complexity of the physics of scattering.

Our study also revealed a positive correlation between the standard deviations of the backscatter and sediment grain size distribution. We were unable to find another example of this comparison in the literature so we cannot conclude whether it is typical for marine sediments. It is possible that the success of the analysis here was because the sediments in Loch Linnhe have a distinct modality, being silty muds with different amounts of sand or gravel. However, we suggest that the analysis presented here could be a useful determinant of grain size sorting.

The use of two different frequencies for bottom characterisation was not conclusive here, mainly because of insufficient ground truth and dual frequency data coverage. Unlike the imaging of the artificial reefs themselves, the results for the two frequencies used here were not noticeably different for the loch sediment. To date, there have not been many dual frequency experiments, the survey most directly comparable to the one presented here being that of Ryan and Flood, 1996. In this earlier study, clear differences in 30 and 75 kHz imagery were detected which were thought to be due to spatial variations in thin sediment cover overlying buried hard ground, and so unfortunately is not directly comparable to our study.

4.2. The use of sidescan in artificial reef projects

In this study, we found sidescan to be an excellent tool for assessing the construction of the artificial reefs. Geographically referenced images of the reef modules of acceptable quality were available in real time, and decisions regarding future block deployments could be made immediately following the survey. For example, one of the reef modules was found to consist of two distinct piles of blocks rather than the expected one, which led to the development of an improved method to position the quarry barge above the site before dropping its cargo. The biggest limitation of the sidescan survey for this object-detection part of the study was the positional uncertainly of ± 20 m. Whilst this did not pose a serious problem at this particular site (as the reef construction was being supported by a team of scientific divers who provided additional positional information), it might at other sites, particularly at one with a more complex design. In such cases, we would recommend clearing the site of obstructions such as seasurface buoys prior to conducting a survey in order to remove any need to make undesirable ship manoeuvres and so improve the positional consistency between the sonar fish and the ship's navigation antenna. To further reduce positional error a pitch/yaw/roll sensor and possibly a local transponder net could be used.

Sidescan sonar has been previously demonstrated to be a useful tool in delineating the boundaries of artificial reefs (Munoz-Perez et al., 2000; Grove et al., 2002; Turpin and Bortone, 2002). However, to our knowledge, there is no published work showing the imaging characteristics with frequency. The poor

definition of the reefs in our 100 kHz remains a mystery, and serves as a reminder of the complexity of the backscattering process. The visual quality of the sonogram obtained over any given artificial reef will be site-specific, as it depends on the contrast of the acoustic properties of the seabed and the construction materials, together with the micro- and macro-relief of the reef. As an alternative to sidescan, swath bathymetry systems have also been used to determine artificial reef morphology (Shyue and Yang, 2002), but these systems are much more costly and logistically more demanding than sidescan.

5. Conclusions

(1) We have developed a method of processing raw sidescan sonar data and extracting statistical information from it for comparison with sediment grain size distributions. The method relies on the application of an empirically derived amplitude-grazing angle correction to the acoustic data. The results showed a positive (r=0.73) correlation between backscatter intensity and mean sediment grain size. We also found a correlation (r=0.59) between the standard deviations of sidescan pixels and sediment grain size, with more heterogeneous sediments giving more variable backscatter intensity measurements. More studies of the type undertaken here are needed to determine whether these results were site-specific or could be applied across a wide-range of environments. However, we suggest that sidescan has great potential for automatic ground discrimination.

(2) There was general agreement between the results of the sidescan sonar survey and a RoxAnn survey. In particular, the RoxAnn index E1 seemed to correlate well with sidescan backscatter intensity, although the latter provided images with much higher spatial detail. The largest source of error in our analysis was probably uncertainty in sonar fish positioning. We suggest that sidescan sonar could be used in tandem with other acoustic methods such as RoxAnn to reduce the number of ground truth stations required to perform robust seabed characterisation.

(3) Imaging of the artificial reefs was highly frequency dependent, with good images obtained at 410 kHz, but poor images at 100 kHz. The reason for this, given the large size of the reef blocks in comparison to both acoustic wavelengths is unknown, and serves as a reminder of the complexity of the backscattering process.

Acknowledgements

We would like to thank the crew of the R/V *Calanus* and Andrew Jephcoat for their help during the collection of the survey data. The GeoAcoustics sidescan sonar used in this project was bought with a 2001 HEFCE-JREI equipment grant JR00IM-COEQ (*Seabed imaging sonars for earth, environment, geohazards, coastal engineering and archaeological research*). This work contributes to the Natural Environment Research Council Connect B grant No: NER/D/S/2000/01307 (*Marine artificial habitat manipulation: prediction and measurement of environmental impacts*). The construction of the Loch Linnhe Artificial Reef was funded by Foster (Morvern). Reviews by Jon Bull and Richard Bates greatly improved an earlier version of this manuscript.

References

Bell, J.M., Chantler, M.J., Wittig, T., 1999. Sidescan sonar: a directional filter of seabed texture? IEE Proc., Radar Sonar Navig. 146, 65–72.

Blondel, P., Murton, B.J., 1997. Handbook of Seafloor Sonar Imagery. Praxis-Wiley and Sons, West Sussex, England, p. 314.

Borgeld, J.C., Clarke, J.E.H., Goff, J.A., Mayer, L.A., Curtis, J.A., 1999. Acoustic backscatter of the 1995 flood deposit on the Eel shelf. Mar. Geol. 154, 197–210.

Boyd, S.E., 2002. Guidelines for the conduct of benthic studies at aggregate dredging sites. Lowestoft, Department for Transport, Local Government and the Regions. CEFAS: 1–117.

Brown, C.J., Cooper, K.M., Meadows, W.J., Limpenny, D.S., Rees, H.L., 2002. Small-scale mapping of sea-bed assemblages in the eastern English Channel using sidescan sonar and remote sampling techniques. Estuar. Coast. Shelf Sci. 54, 263–278.

Burns, D., Queen, C.B., Chivers, R.C., 1985. An ultrasonic signal processor for use in underwater acoustics. Ultrasonics 23, 189–191.

Cervenka, P., de-Moustier, C., 1993. Sidescan sonar image processing techniques. IEEE J. Oceanic Eng. 18, 108–122.

Chavez, P.S., 1986. Processing techniques for digital sonar images from Gloria. Photogramm. Eng. Remote Sensing 52, 1133–1145.

Chivers, R.C., Emerson, N., Burns, D.R., 1990. New acoustic processing for underway surveying. Hydrogr. J. 56, 9–17.

Collins, M.B., Voulgaris, G., 1993. Empirical field and laboratory evaluation of a real-time acoustic seabed survey system. Proc. Inst. Acoust. 15, 343–351.

Davis, K.S., Slowey, N.C., Stender, I.H., et al., 1996. Acoustic backscatter and sediment textural properties of inner shelf sands, northeastern Gulf of Mexico. Geo-Mar. Lett. 16, 273–278.

Edwards, B.D., Dartnell, P., Chezar, H., 2003. Characterizing benthic substrates of Santa Monica Bay with seafloor photography and multibeam sonar imagery. Mar. Environ. Res. 56, 47–66.

Fonseca, L., Mayer, L., Orange, D., Driscoll, N., 2002. The high-frequency backscattering angular response of gassy sediments: model/data comparison from the Eel River Margin, California. J. Acoust. Soc. Am. 111, 2621–2631.

Foster-Smith, R.L., Sotheran, I.S., 2003. Mapping marine benthic biotopes using acoustic ground discrimination systems. Int. J. Remote Sens. 24, 2761–2784.

Fyfe, J.A., Long, D., Evans, D., 1993. United Kingdom offshore regional report: the geology of the Malin–Hebrides sea area. HMSO for the BGS, p. 91.

Gardner, J.V., Field, M.E., Lee, H., et al., 1991. Ground-truthing 6.5 kHz side scan sonographs: what are we really imaging? J. Geophys. Res. 96, 5955–5974.

Goff, J.A., Olson, H.C., Duncan, C.S., 2000. Correlation of side-scan backscatter intensity with grain-size distribution of shelf sediments, New Jersey margin. Geo-Mar. Lett. 20, 43–49.

Greenstreet, S.P.R., Tuck, I.D., Grewar, G.N., et al., 1997. An assessment of the acoustic survey technique, RoxAnn, as a means of mapping seabed habitat. ICES J. Mar. Sci. 54, 939–959.

Grove, R.S., Zabloudil, K., Norall, T., Deysher, L., 2002. Effects of El Nino events on natural kelp beds and artificial reefs in southern California. ICES J. Mar. Sci. 59, S330–S337.

Hamilton, L.J., Mulhearn, P.J., Poeckert, R., 1999. Comparison of RoxAnn and QTC-View acoustic bottom classification system performance for the Cairns area, Great Barrier Reef, Australia. Cont. Shelf Res. 19, 1577–1597.

Hughes-Clarke, J., 1994. Towards remote seafloor classification using the angular response of acoustic backscattering: a case study from multiple overlapping GLORIA data. IEEE J. Oceanic Eng. 19, 112–127.

Humber, S., 2003. High-resolution side-scan sonar imaging of coral reefs in the Seychelles. PhD thesis, Department Earth Science and Engineering, Imperial College, University of London.

Huvenne, V.A.I., Blondel, P., Henriet, J.-P., 2002. Textural analysis of sidescan sonar imagery from two mound provinces in the Porcupine Seabight. Mar. Geol. 189, 323–341.

Jackson, D.R., Baird, A.M., Crisp, J.J., Thomson, P.A.G., 1986. High-frequency bottom backscatter measurements in shallow water. J. Acoust. Soc. Am. 80, 1188–1199.

Jackson, D.R., Williams, K.L., Thorsos, E.I., Kargl, S.G., 2002. High-frequency subcritical acoustic penetration into a sandy sediment. IEEE J. Oceanic Eng. 27, 346–361.

Johnson, H.P., Helferty, M., 1990. The geological interpretation of side-scan sonar. Rev. Geophys. 28, 357–380.

Knebel, H.J., Signell, R.P., Rendigs, R., Poppe, L.J., List, J.H., 1999. Seafloor environments in the Long Island Sound estuarine system. Mar. Geol. 155, 277–305.

Munoz-Perez, J.J., Mas, J.M.G., Naranjo, J.M., Torres, E., Fages, L., 2000. Position and monitoring of anti-trawling reefs in the Cape of Trafalgar (Gulf of Cadiz, SW Spain). Bull. Mar. Sci. 67, 761–772.

Pace, N.G., Gao, H., 1988. Swathe seabed classification. IEEE J. Oceanic Eng. 13, 83–90.

Pinn, E.H., Robertson, M.R., 2003. Effect of track spacing and data interpolation on the interpretation of benthic community distributions derived from RoxAnn (TM) acoustic surveys. ICES J. Mar. Sci. 60, 1288–1297.

Ryan, W.B.F., Flood, R.D., 1996. Side-looking sonar backscatter response at dual frequencies. Mar. Geophys. Res. 18, 689–705.

Sayer, M.D.J., Wilding, T.A., 2002. Planning, licensing, and stakeholder consultation in an artificial reef development: the Loch Linnhe reef, a case study. ICES J. Mar. Sci. 59, S178–S185.

Schlagentweit, G.E.O., 1993. Real-time acoustic bottom classification. A field evaluation of RoxAnn. Oceans 93, 214–219.

Shennan, I., 1989. Holocene crustal movements and sea-level changes in Great Britain. J. Quat. Sci. 4, 77–89.

Shyue, S.W., Yang, K.T., 2002. Investigating terrain changes around artificial reefs by using a multi-beam echosounder. ICES J. Mar. Sci. 59, S338–S342.

Smith, W.H.F., Wessel, P., 1990. Gridding with continuous curvature splines in tension. Geophysics 55, 293–305.

Somers, M.L., Stubbs, A.R., 1984. Sidescan sonar. IEE Proc. F, Commun. Radar Signal Process. 131, 243–256.

Sotheran, I.S., Foster-Smith, R.L., Davies, J., 1997. Mapping of marine benthic habitats using image processing techniques within a raster-based geographic information system. Estuar. Coast Shelf Sci. 44, 25–31.

Stanton, T.K., 1984. Sonar estimates of seafloor microroughness. J. Acoust. Soc. Am. 75, 809–818.

Sternlicht, D.D., de-Moustier, C.P., 2003. Time-dependent seafloor acoustic backscatter (10–100 kHz). Acoust. Soc. Am. 114, 2709–2725.

Turpin, R.K., Bortone, S.A., 2002. Pre- and post-hurricane assessment of artificial reefs: evidence for potential use as refugia in a fishery management strategy. ICES J. Mar. Sci. 59, S74–S82.

Urgeles, R., Locat, J., Schmitt, T., Clarke, J.E.H., 2002. The July 1996 flood deposit in the Saguenay Fjord, Quebec, Canada: implications for sources of spatial and temporal backscatter variations. Mar. Geol. 184, 41–60.

Urick, R.J., 1967. Principles of Underwater Sound for Engineers. McGraw-Hill Book.

Wessel, P., Smith, W.H.F., 1991. Free software helps map and display data. EOS Tans. AGU 71, 441.

Wilding, T.A., Sayer, M.D.J., 2002. Evaluating artificial reef performance: approaches to pre- and post-deployment research. ICES J. Mar. Sci. 59, S222–S230.

Williams, K.L., Jackson, D.R., Thorsos, E.I., Tang, D., Briggs, K.B., 2002. Acoustic backscattering experiments in a well characterised sand sediment: data/model comparisons using sediment fluid and Biot models. IEEE J. Oceanic Eng. 27, 376–387.